Single step deposition method for nearly stoichiometric $CuInSe_2$ thin films.

Sreejith Karthikeyan[a*], Arthur E Hill[a], Richard D Pilkington [a], John S Cowpe [a], Jörg Hisek [b] and Darren M Bagnall [c].

[a] Materials and Physics Research Centre, University of Salford, Salford, M5 4WT, UK

[b] Technische Universität Braunschweig, Hannover, Germany

[C] School of Electronics and Computer Science, University of Southampton, SO17 1BJ, UK

[*]**Corresponding author**: s.karthikeyan@edu.salford.ac.uk

Abstract

This paper reports the production of high quality copper indium diselenide thin films using pulsed DC magnetron sputtering from a powder target. As–grown thin films consisted of pin-hole free, densely packed grains. X–ray diffraction showed that films were highly orientated in the (112) and/or (204)/(220) direction with no secondary phases present. The most surprising and exciting outcome of this study was that the as-grown films were of near stoichiometric composition, almost independent of the composition of the starting material. No additional steps or substrate heating were necessary to incorporate selenium and create single phase $CuInSe_2$. Electrical properties obtained by hot point probe and four point probe gave values of low resistivity and showed that the films were all p–type. The physical and structural properties of these films were analyzed using x-ray diffraction, scanning electron microscopy and atomic force microscopy. Resistivity measurements were carried out using the four point probe and hot probe methods. The single step deposition process can cut down the cost of the complex multi step processes involved in the traditional vacuum based deposition techniques.

Keywords

$CuInSe_2$ thin films, pulsed DC magnetron sputtering, stoichiometric $CuInSe_2$ films, photovoltaic, solar cells, single step $CuInSe_2$ films.

1. Introduction

Copper indium diselenide (CIS) is one of the most promising materials for high efficiency thin film photovoltaic devices. Its high absorption coefficient, low toxicity, and electrical and optical properties make this compound a major candidate for the next generation of solar cells. Because of this high potential, researchers have developed a variety of techniques to deposit CIS thin films such as flash evaporation [1] [2], co-evaporation [3], sputtering[4] [5], molecular beam epitaxy [6], spray pyrolysis [7] [8], chemical vapour deposition [9] , etc. Many of these require a potentially dangerous post selenization process [10-12]. The use of H_2Se during selenization requires extensive health and safety measures and can introduce secondary phase formations such as In_2Se which will degrade the properties of the CIS films [13]. A relatively cheap and eco-friendly method was introduced with chemical bath deposited Se by Bindu et al., and Deepa et al., [14, 15] but this method also requires a multi step processes. These processes are complex and controlling the deposition parameters reproducibly is a difficult task. It is the aim of continued research to find a simplified method that will allow the deposition of stoichiometric CIS thin films using a single stage process capable of producing large area device quality material.

This work describes the single step deposition of near stoichiometric $CuInSe_2$ films from a polycrystalline powdered target using the Pulsed DC Magnetron Sputtering (PDMS) process in the mid frequency region (10 to 350 kHz). Pulsed DC. sputtering alleviates the charging problems associated with R.F sputtering and continuous DC sputtering. This is achieved by the production of a stable sputtering plasma during the *pulse on* time and discharge of the charged regions on the target during the reverse voltage or *pulse off* time. PDMS has been used to deposit dielectric materials in a long-term arc free environment,[16] which has proved difficult using other sputtering techniques The quality of the deposited films can be adjusted using various parameters such as frequency, duty cycle, voltage, current etc. The optimum choice of these can result in coatings with the desired characteristics.

2. Experimental details

2.1. Crystal Growth

Polycrystalline CIS crystals were made by the direct fusion method from the component elements using a rocking furnace. Copper, indium and selenium of 99.999 % purity were used for all the experiments. The base elements were sealed inside a cleaned, dry quartz ampoule under vacuum. The sealed ampoules were heated and cooled inside a rocking furnace controlled by a Eurotherm programmable temperature controller. The rocking mechanism ensured the homogeneity of the mixing process.

The temperature of the furnace was pre-programmed as follows.

Heating

$0\ ^{o}C \rightarrow 100\ ^{o}C$: 5.0 ^{o}C / minute

$100\ ^{o}C \rightarrow 300\ ^{o}C$: 0.5 ^{o}C /minute

$300\ ^{o}C \rightarrow 1150\ ^{o}C$: 10.0 ^{o}C / minute (kept at 1150 ^{o}C for 2 hrs)

Cooling

$1150\ ^{o}C \rightarrow 0\ ^{o}C$: 10 ^{o}C / minute

This stepped heating programme is necessary for the growth of $CuInSe_2$ because care is needed between 100 ^{o}C and 300 ^{o}C due to an exothermic reaction between selenium and indium. The heating programme ensures complete reaction of the base elements and minimizes the risk of ampoule explosion.[17-19]. Figure 1 shows the base elements and the resulting polycrystalline CIS. Various atomic compositions of CIS were grown. Crystals were then powdered for use as sputtering targets.

2.2. Pulsed DC Magnetron Sputtering System

The schematic of the pulsed DC magnetron apparatus is shown in Figure 2. The system consisted of a cylindrical stainless steel vacuum chamber, pumped with a turbo molecular pump backed by a rotary pump. A two-inch unbalanced circular magnetron served as the target head using the powdered polycrystalline CIS as the target source. The powder was compressed inside the circular recess of the target holder. An Advanced Energy Pinnacle

Plus pulsed DC. power supply operated in constant current mode was used to supply power to the cathode. The system pressure was monitored using a capacitance manometer pressure gauge. The system was pumped to obtain an acceptable base pressure of 5.5 $x10^{-4}$ Pa. The operating pressure of 7.5 x 10^{-1} Pa was set and controlled using a 100 sccm range MKS argon mass flow controller controlled by an MKS multi gas controller model 147. Films were deposited on glass microscope slides that had been cleaned using isopropyl alcohol and acetone in an ultrasonic bath.

The films were grown from powders with different starting atomic ratios. The surface morphology and the atomic percentage of the individual base elements were analysed using a Philips XL 30S scanning electron microscope (SEM) equipped with an EDX (Energy-dispersive X-ray spectroscopy) detector unit. An EDAX Phoenix x-ray microanalysis system with a Super Ultra-thin window sapphire detector was used for EDX analysis. The accelerating voltage for the SEM and EDX measurements was set to 15kV. The life time count was set to 100 seconds for the EDX measurements. The type of electrical conductivity was established using the hot point probe method and resistivity measurements were carried out with a four point probe. The surface profile and roughness were analysed using a Veeco diCaliber atomic force microscope (AFM), operated in tapping mode at 241.65 kHz with a sharp silicon tip (maximum radius of 12 nm). The thickness measurements were performed using a Dektak 3M profilometer and cross sectional views of films were measured from SEM images. The structural characterisation was carried out with a SIMENS D5000 x-ray diffractometer (XRD) with a CuKα (λ =1.5405 Å) radiation. The powder was analysed using locked coupled mode (2θ from 10 to 90) and the films were analysed using a detector scan (2θ from 10 to 60).

3. Results and Discussion

3.1. Polycrystalline $CuInSe_2$ powder

Polycrystalline $CuInSe_2$ ingots with different compositions were analysed using EDX to obtain the atomic percentages tabulated in Table 1. The samples were taken from three

different positions along the length of the ingot. It was found that the composition was nearly the same for all the positions from the same batch. This verified the uniformity of the samples throughout the ingot and testifies to the efficiency of the rocking technique. Results are also shown for one batch of previously prepared $CuInSe_2$ powder (CISRF00H). The deviation from the stoichiometric composition can be explained with the help of two parameters, Δm and Δs, from the intrinsic defect model. Δm refers to the deviation from molecularity and Δs refers to the deviation from valance stoichiometry [20].

$$\Delta m = \frac{[Cu]}{[In]} - 1 \qquad (1)$$

$$\Delta s = \frac{2[Se]}{[Cu] + 3[In]} - 1 \qquad (2)$$

If both parameters are zero then there is no deviation and the material is perfectly stoichiometric. If they are not zero:

1. $\Delta m > 0 \Leftrightarrow$ Cu rich film

   $\Delta m < 0 \Leftrightarrow$ In rich film

2. $\Delta s > 0 \Leftrightarrow$ Selenium excess

   $\Delta s < 0 \Leftrightarrow$ Selenium deficient

The crystals were carefully ground into powder and the structural properties of the powdered samples were analyzed using a SIEMENS D 5000 x-ray diffractometer in locked couple mode, as shown in Figure 3.

The peak position of sample CISRF006 exactly matches with the JCPDS data for $CuInSe_2$ (CAS No: 40-1487). The selenium rich CISRF007 has extra low intensity peaks at 2θ of 23.64^o and 29.71^o. The indium rich CISRF009 has a peak at 2θ of 21.27^o but there is no data available to match this point. The chalcopyrite characteristic lines (101) at 17.15^o, (103) at 27.70^o and (211) at 35.5^o are present in all the samples. These peaks verify that the crystals are in the α- phase [21].

The lattice parameters *a* and *c* of the tetragonal structure are calculated using equation (3) and tabulated in Table 2.

$$\frac{1}{d^2} = \frac{h^2 + k^2}{a^2} + \frac{l^2}{c^2} \qquad (3)$$

where hkl are Miller indices , d is the inter-planar spacing

The inter-planar spacing *d* and the Miller indices can be determined from the diffractogram. In order to determine the *a* and *c* values, at least two reflections are needed and the corresponding equations are solved using Cramer's rule. Calculations were carried out with the (101), (112) and (211) peaks: these peaks were fitted using a Lorentzian function for the accurate 2θ value. The mean values of *a* and *c* from each analysis are given in Table 2. The tetragonal distortion parameter $\eta = c/2a \neq 1$ is also calculated and tabulated in the same table. The distortion parameter is slightly different for the Se rich CISRF007 sample. The other values are near to the previously reported value of 1.003 - 1.008 [22, 23] **3.2. $CuInSe_2$ thin films**

Two sets of films were deposited from each powder with different sputtering times. The power supply was operated in constant current mode at 0.12 A. The frequency was set to 130 kHz with a pulse off time of 1 µs. The operating parameters are listed in Table 3.

The XRD structural analysis revealed the presence of three prominent peaks corresponding to the planes (112), (220/204), (116)/(312) at 2θ equal to 26.6^o, 44.1^o and 52.3^o respectively, (Figure 4). A (301) peak at 47.87^o was observed for samples made from indium rich powder, which was additional to the above stated planes (JCPDS 40-1487). The lattice parameters and the tetragonal distortion factors were calculated from the prominent peaks and average value tabulated in Table 4.

The tetragonal distortion factors were found to be <1. This is slightly less than the reported value of 1.004 [23]. This is due to the difficulty in distinguishing the peak positions from the (220/204) and (116/312) planes. The value of η is consistent to the second decimal place for all the films and suggests that the tetragonal distortion of the grown film is

independent of the starting powder combination. This is especially true for samples CIST113 and CIST114 deposited from CISRF007 with an η value of 1.0138. The crystalline size was calculated using the Debye-Scherrer equation and indicates that the thicker sample (Table 5) has a greater crystalline size.

The atomic percentages of the films were analyzed using EDX. The point defect model parameters, Δm and Δs, were calculated using the atomic percentages from Equations 1 and 2 as tabulated in Table 4. The conductivity type was determined with the hot point probe method. Interestingly, all the samples were shown to have p- type conductivity. A systematic study was carried out by Neumann and Tomlinson on the relationship in CIS single crystals between the electrical properties and the composition [24]. They analyzed 104 n-type and 76 p-type crystals near to the stoichiometric ratio, with $|\Delta m| < 0.08$ and $|\Delta s| < 0.06$. They found that those crystals with $\Delta s > 0$ and $\Delta m > 0$ were always p-type and those crystals with $\Delta s < 0$ and $\Delta m <> 0$, were n-type. But they did not report any samples in which $\Delta s > 0$ and $\Delta m < 0$. Their second series of measurements was based on crystals with a larger deviation from stoichiometry and they found that the point defect model fails in this region. The samples with $\Delta m > 0$ and $\Delta s > 0$ were again always p-type but samples with $\Delta m < 0$ and $\Delta s <> 0$ were always n-type. Another interesting classification was in a range corresponding to $\Delta m > 0$ and $\Delta s < 0$ where they randomly observed both p-type and n-type conductivity. Comparing these results with our samples reveals that our results are closer to Neumann and Tomlinson's first group near to stoichiometric composition, even though our maximum Δs is 0.15. However, four of our films, CIST104, CIST105, CIST113 and CIST114, had $\Delta m < 0$ and $\Delta s > 0$ and there is no such classification in the cited work [24]. There could be two possible explanations. Taking account of the 1% EDX error there is a possibility that Δm can change its apparent value to positive. Secondly, the work done by Albin et al., [25] suggests the importance of the Δs value in causing a change in the Fermi level and hence the electronic defect distribution. This finding indicates that a small selenium excess always

results in a p-type characteristic. p-type CIS thin film based solar cells have always been shown to have a higher efficiency compared with corresponding n-type based cells [26].

The starting powder compositions and corresponding final film compositions were compared with the help of a ternary diagram, shown in Figure 5. This illustrates the observation that the films' composition is largely independent of the starting powder atomic composition and that the resulting films were nearly stoichiometic. This significant result underlines the importance of employing pulsed D.C. magnetron sputtering as a single step process that can produce the desired p-type CIS films with nearly stoichometric compositions without an associated selenization process.

The thickness of the samples was measured using a Dektak profilometer and also using SEM cross sections for samples CIS105, 111, 114 and 116. The difference in thicknesses measurement between the two techniques was ± 30nm. The corresponding resistivities are listed in Table 5. The lowest resistivity values were observed for the films grown from nearly stoichiometric powder.

The surface morphology of the samples was analyzed by SEM (Figure 6) and AFM (Figure 7). The SEM was operated with 15 kV accelerating voltage. The morphological features were analyzed in secondary electron mode and compared with 100000x magnification. The cross sections were taken in back scattered electron mode with 20000x magnification. The AFM images were taken in tapping mode. The images of three samples sputtered from different powders are shown in Figure 6. A cross sectional view and grain size histogram of sample CIST116 are also shown. The histogram was generated by calculating the individual particle sizes of 50 particles that were close to each other in the AFM image in order to obtain a general over-view of the particle size distribution. The particle sizes varied from 90 nm to 329 nm. Larger particle sizes were obtained from CIST111 and CIST116 which were deposited from the stoichiometric powder and indium rich powder, respectively. The average particle size of the samples was in the 180-210 nm band. The SEM image also

showed that the films deposited from the stoichiometric powder and indium rich powder exhibited the largest particle size.

The roughness of the samples was calculated and sample (CIST111) that was deposited from nearly stoichiometric powder (CISRF006) showed the lowest roughness value of 4.42 nm. The maximum roughness value of 7.83 nm was observed for sample (CIST114) grown from selenium rich powder (CISRF007). The samples from the indium rich films had roughness values of 5.24 nm (CIST105) and 7.63 nm (CIST116). The SEM analysis shows some angular structure in the particles and hexagonal, pentagonal and triangular shapes are clearly visible. The cross sectional image shows the columnar growth of the film.

4. Conclusion

$CuInSe_2$ films were deposited from polycrystalline powders of different atomic compositions using a single step pulsed DC magnetron sputtering process at room temperature. XRD analysis shows that films have preferred growth in the (112) direction. Tetragonal distortion of the grown film is independent of the starting powder combination. All the films were shown to exhibit p-type conductivity and were pin-hole free. Films were found to be near stoichiometric, largely irrespective of the starting composition of the material. The average grain size of 180-210 nm was obtained from AFM images. The lowest roughness value was obtained for the films which were deposited from stoichiometric powder. The near stoichometric nature of the films grown from this single step process can cut down the cost and the use of a post deposition selenization process. Another advantage of this technique is the use of powdered targets, which avoids the cost of making solid CIS targets using a hydraulic press. Future work will aim to improve the sputtering rate with an improved target holder design and also study the electrical and optical properties of these films as a function of different substrate heating and biasing conditions.

Acknowledgement

The authors gratefully acknowledge the Joule Centre for the funding of this project. Sincere thanks are due to the Higher Education Funding Council for England (HEFCE) for the award of a research fellowship to Sreejith Karthikeyan under the ORSAS programme. The authors gratefully acknowledge Dr. J.Hinks, Materials and Physics Research Centre, University of Salford for his expert guidance in preparing the CIS crystals.

References

[1] R. Durný, A.E. Hill, R.D. Tomlinson, Thin Solid Films 69 (1980) L11.
[2] G. Salviati, D. Seuret, Thin Solid Films 104 (1983) L75.
[3] A. Amara, A. Ferdi, A. Drici, J.C. Bernède, M. Morsli, M. Guerioune, Catal. Today 113 (2006) 251.
[4] A. Rockett, T.C. Lommasson, P. Campos, L.C. Yang, H. Talieh, Thin Solid Films 171 (1989) 109.
[5] J. Piekoszewski, J.J. Loferski, R. Beaulieu, J. Beall, B. Roessler, J. Shewchun, Sol. Energy Mater. Sol. Cells 2 (1980) 363.
[6] S. Niki, Y. Makita, A. Yamada, O. Hellman, P.J. Fons, A. Obara, Y. Okada, R. Shioda, H. Oyanagi, T. Kurafuji, S. Chichibu, H. Nakanishi, J. Cryst. Growth 150 (1995) 1201.
[7] K. Subbaramaiah, V. Sundara Raja, Thin Solid Films 208 (1992) 247.
[8] B. Pamplin, R.S. Feigelson, Thin Solid Films 60 (1979) 141.
[9] P.A. Jones, A.D. Jackson, P.D. Lickiss, R.D. Pilkington, R.D. Tomlinson, Thin Solid Films 238 (1994) 4.
[10] A.V. Mudryi, V.F. Gremenok, I.A. Victorov, V.B. Zalesski, F.V. Kurdesov, V.I. Kovalevski, M.V. Yakushev, R.W. Martin, Thin Solid Films 431-432 (2003) 193.
[11] J. Bekker, V. Alberts, M.J. Witcomb, Thin Solid Films 387 (2001) 40.
[12] H.K. Song, S.G. Kim, H.J. Kim, S.K. Kim, K.W. Kang, J.C. Lee, K.H. Yoon, Sol. Energy Mater. Sol. Cells 75 (2003) 145.
[13] S. Deok Kim, H.J. Kim, K. Hoon Yoon, J. Song, Sol. Energy Mater. Sol. Cells 62 (2000) 357.
[14] K. Bindu, C.S. Kartha, K.P. Vijayakumar, T. Abe, Y. Kashiwaba, Sol. Energy Mater. Sol. Cells 79 (2003) 67.
[15] K.G. Deepa, P.M. Ratheesh Kumar, C. Sudha Kartha, K.P. Vijayakumar, Sol. Energy Mater. Sol. Cells 90 (2006) 3481.
[16] P.J. Kelly, R.D. Arnell, J. Vac. Sci. Technol., A 16 (1998) 2858.
[17] J. Parkes, R.D. Tomlinson, M.J. Hampshire, J. Cryst. Growth 20 (1973) 315.
[18] H. Matsushita, T. Takizawa, J. Cryst. Growth 160 (1996) 71.
[19] G. Kühn, U. Boehnke, J. Cryst. Growth 61 (1983) 415.
[20] J.A. Groenik , P.H. Janse, Z. Phys. Chem 110 (1978) 17.
[21] M. Lachab, A.A. Attia, C. Llinarès, J. Cryst. Growth 280 (2005) 474.
[22] M. Fearheiley, K. Bachmann, Y. Shing, S. Vasquez, C. Herrington, J. Electron. Mater. 14 (1985) 677.
[23] J.E. Jaffe, A. Zunger, Phys. Rev. B: Condens. Matter 28 (1983) 5822.
[24] H. Neumann, R.D. Tomlinson, Solar Cells 28 (1990) 301.
[25] D. Albin, R. Noufi, J. Tuttle, J. Goral, S.H. Risbud, J. Appl. Phys. 64 (1988) 4903.
[26] D. Haneman, Crit. Rev. Solid State Mater. Sci. 14 (1988) 377.

Table Captions

Table 1. EDX results of $CuInSe_2$ polycrystals.

Table 2. Lattice parameter and tetragonal distortion parameter of the starting powder.

Table 3. Operating parameters of the sputtered samples.

Table 4. Lattice parameter, tetragonal distortion and crystalline size of sputtered films.

Table 5. Compositional and conductivity analysis of CIS films.

Figure captions.

Figure 1. (a) Base elements before reaction (b) CIS crystals inside ampoule after reaction (c) CIS crystals after removal from ampoule.

Figure 2. Schematic of pulsed DC magnetron sputtering system.

Figure 3. The x-ray diffraction spectra of $CuInSe_2$ powder.

Figure 4. The x-ray diffraction spectra of $CuInSe_2$ films.

Figure 5. Ternary graph of the starting powder compositions and the final film composition.

Figure 6. SEM images of $CuInSe_2$ films (a) from nearly stoichiometric powder (b) from Se rich powder (c) from In rich powder (d) cross sectional view of CIST116.

Figure 7. AFM images of $CuInSe_2$ films (a) from nearly stoichiometric powder (b) from Se rich powder (c) from In rich powder (d) cluster size histogram generated from CIST116 sample.

Tables 1

Sample Name	Mixing Percentage	Atomic Persentage (EDX)			Δm	Δs
		Cu%	In%	Se %		
CISRF007	Unknown	19.95	34.10	45.95	-0.415	-0.248
CISRF009	25:25:50	23.02	23.32	53.66	-0.013	0.154
CISRF007	5% extra Se	21.54	24.29	54.17	-0.113	0.148
CISRF00H	5% extra In	20.53	27.97	51.50	-0.266	-0.138

Tables 2

Sample Name	a (Å)	c (Å)	η=c/2a
CISRF006	5.755	11.565	1.005
CISRF007	5.800	11.760	1.014
CISRF009	5.815	11.665	1.003
CISRF00H	5.790	11.610	1.003

Tables 3

Sample Name	Starting Material	Voltage (V)	Power (W)	Time (hr)
CIST104	CISRF00H	385	45	4
CIST105	CISRF00H	384	45	5
CIST111	CISRF006	358	43	5
CIST112	CISRF006	352	42	4
CIST113	CISRF007	364	44	4
CIST114	CISRF007	365	44	5
CIST115	CISRF009	368	44	4
CIST116	CISRF009	370	44	5

Tables 4

Sample Name	a(Å)	c (Å)	η=c/2a	Crystalline size (nm)
CIST104	5.820	11.629	0.999	12.54
CIST105	5.827	11.615	0.997	12.89
CIST112	5.796	11.579	0.999	11.60
CIST111	5.808	11.582	0.997	14.62
CIST113	5.827	11.615	0.997	11.11
CIST114	5.811	11.589	0.997	12.85
CIST115	5.825	11.638	0.999	14.64
CIST116	5.830	11.625	0.997	19.22

Tables 5

Sample Name	Atomic Percentage (EDX)			Δm	Δs	Thickness	Resistivity (ρ)
	Cu%	In%	Se %			(μm)	Ω cm
CIST104	23.03	23.48	53.49	-0.0192	0.1445	0.921	0.0892
CIST105	22.06	24.15	53.79	-0.0865	0.1383	1.203	0.0823
CIST111	23.97	23.62	52.41	0.0148	0.1053	1.170	0.0321
CIST112	24.32	23.43	52.25	0.0380	0.1045	0.872	0.0379
CIST113	21.97	23.78	54.25	-0.0761	0.1628	1.440	0.0520
CIST114	22.66	23.62	53.72	-0.0406	0.1488	1.750	0.0469
CIST115	24.78	22.98	52.24	0.0783	0.1148	1.330	0.0620
CIST116	24.40	23.22	52.38	0.0508	0.1138	1.730	0.0526

Figure 1
Click here to download Figures (if any): Figure 1.ppt

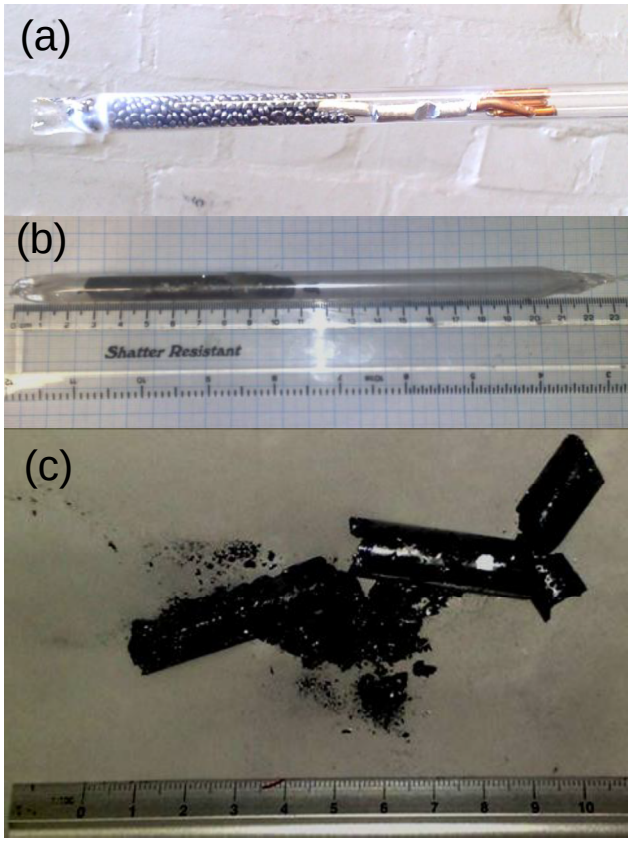

Figure 2

Click here to download Figures (if any): Figure 2.ppt

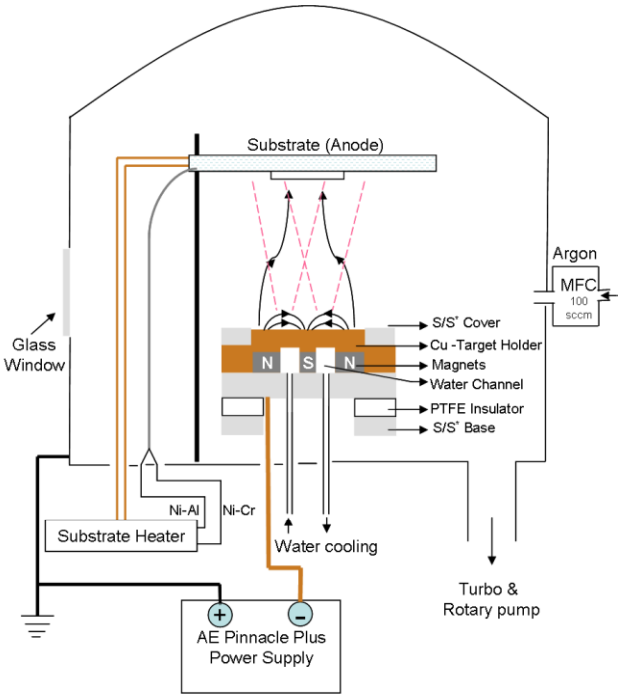

Figure 3
Click here to download Figures (if any): Figure 3.ppt

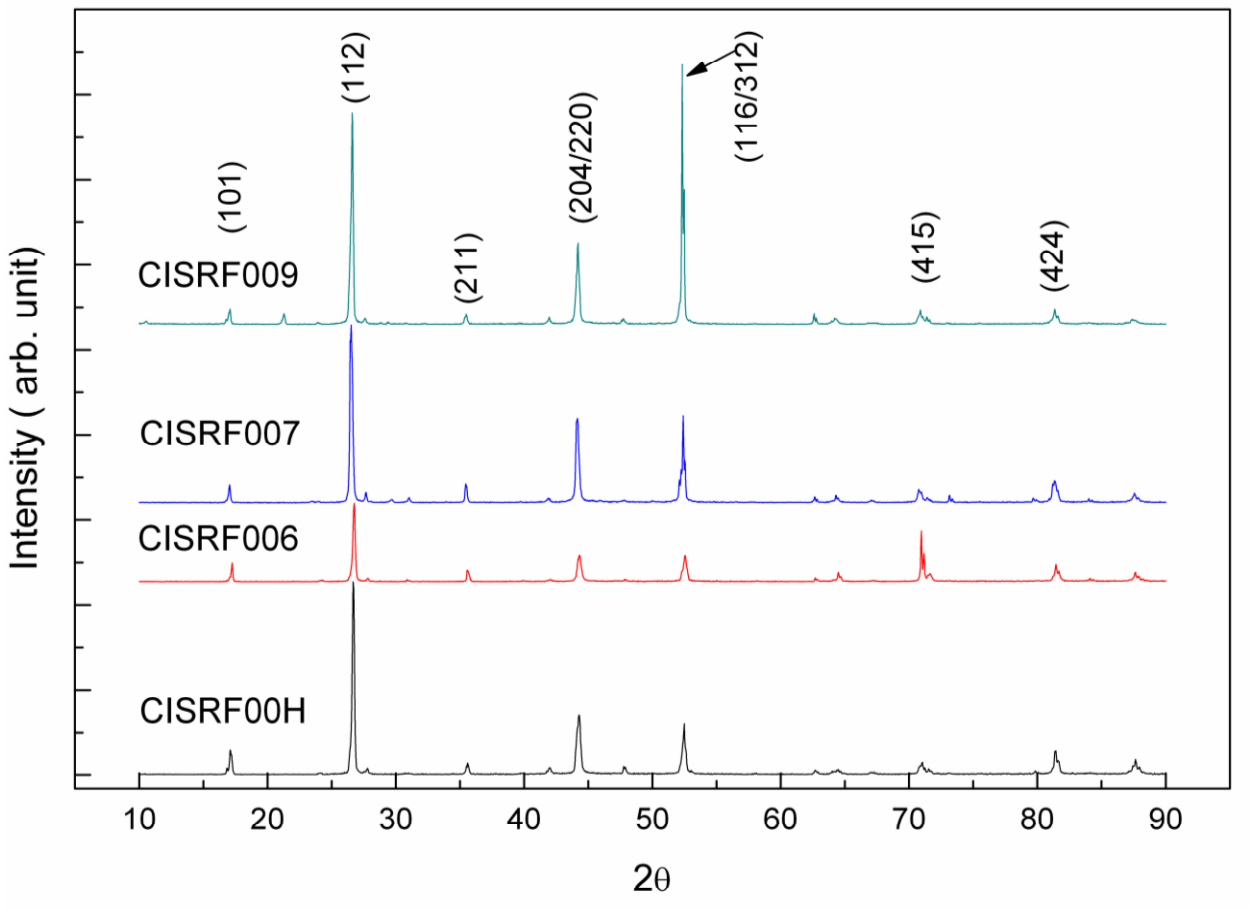

Figure 4

Click here to download Figures (if any): Figure 4.ppt

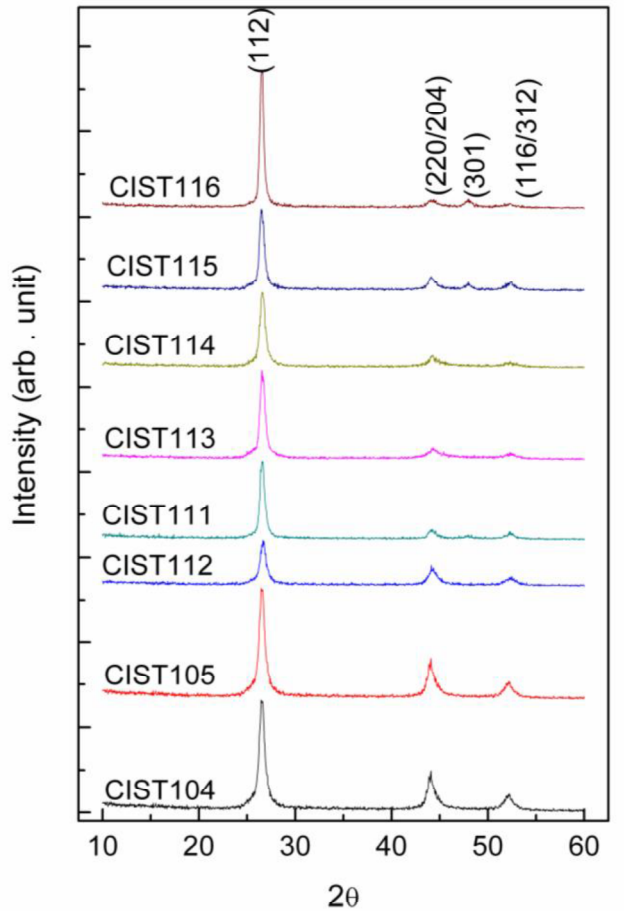

Figure 5

Click here to download Figures (if any): Figure 5.ppt

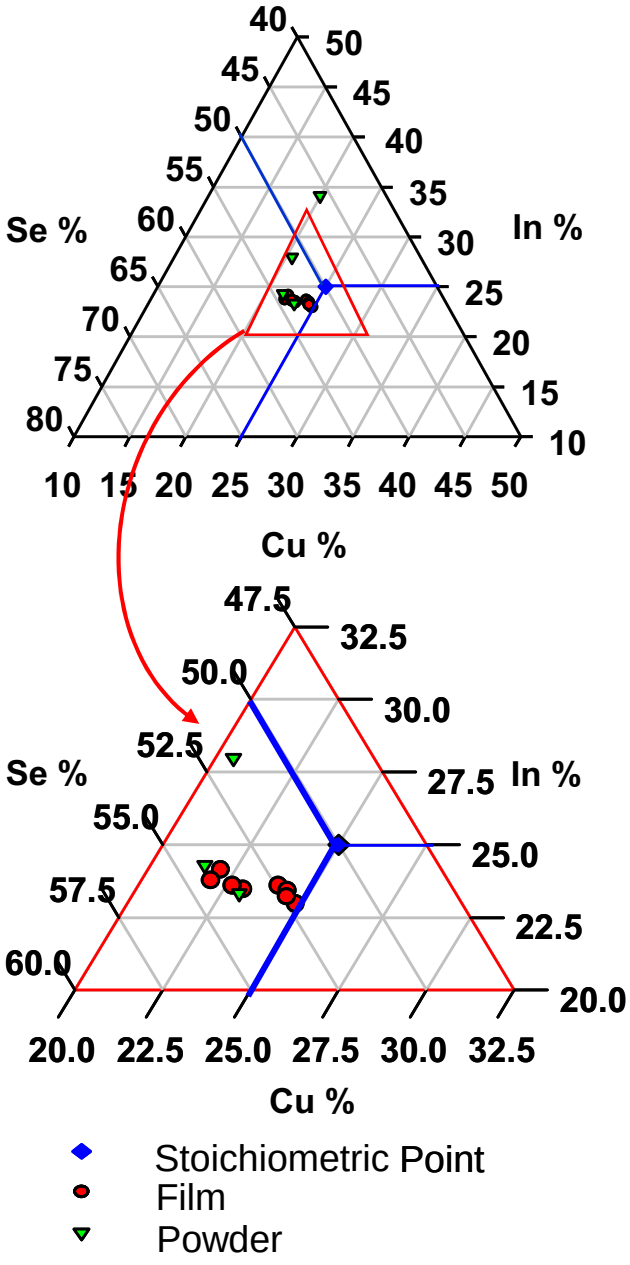

Figure 6

Click here to download Figures (if any): Figure 6.ppt

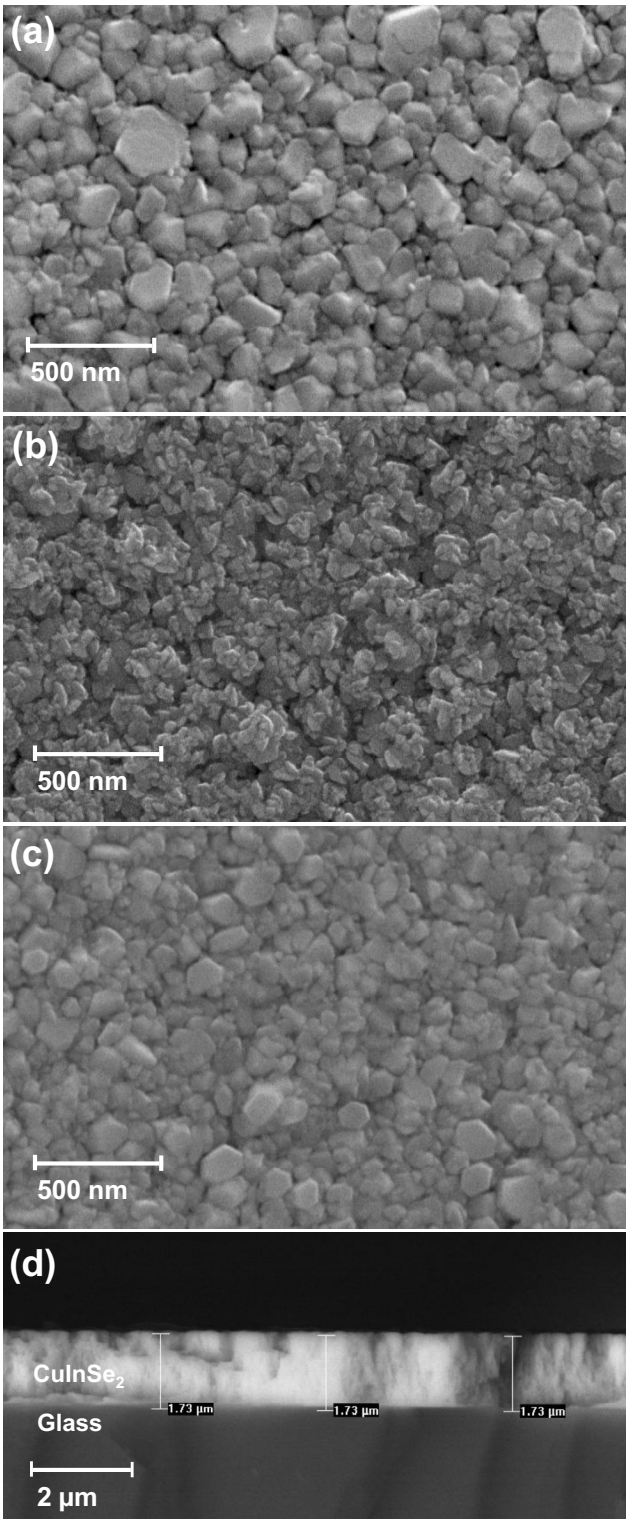

Figure 7

Click here to download Figures (if any): Figure 7.ppt